

A System-Based Approach to Modeling the Ultrasound Signal Backscattered by Red Blood Cells

Isabelle Fontaine,* Michel Bertrand,^{#§} and Guy Cloutier*[#]

*Laboratory of Biomedical Engineering, Institut de Recherches Cliniques de Montréal; [#]Institute of Biomedical Engineering, École Polytechnique de Montréal and Faculty of Medicine, Université de Montréal; and [§]Institut de Cardiologie de Montréal, Montréal, Québec, Canada

ABSTRACT A system-based model is proposed to describe and simulate the ultrasound signal backscattered by red blood cells (RBCs). The model is that of a space-invariant linear system that takes into consideration important biological tissue stochastic scattering properties as well as the characteristics of the ultrasound system. The formation of the ultrasound signal is described by a convolution integral involving a transducer transfer function, a scatterer prototype function, and a function representing the spatial arrangement of the scatterers. The RBCs are modeled as nonaggregating spherical scatterers, and the spatial distribution of the RBCs is determined using the Percus-Yevick packing factor. Computer simulations of the model are used to study the power backscattered by RBCs as a function of the hematocrit, the volume of the scatterers, and the frequency of the incident wave (2–500 MHz). Good agreement is obtained between the simulations and theoretical and experimental data for both Rayleigh and non-Rayleigh scattering conditions. In addition to these results, the renewal process theory is proposed to model the spatial arrangement of the scatterers. The study demonstrates that the system-based model is capable of accurately predicting important characteristics of the ultrasound signal backscattered by blood. The model is simple and flexible, and it appears to be superior to previous one- and two-dimensional simulation studies.

INTRODUCTION

Although ultrasonography is a well-established noninvasive technique for the diagnosis of circulatory diseases, it still has a great potential for new developments. In particular, the information contained in the signal backscattered by red blood cells (RBCs) remains largely unexploited. Because of the very dense suspension of scatterers in normal blood (Mo and Cobbold, 1992), the characteristics of the ultrasound signal backscattered by RBCs are determined by complex wave interactions. Several studies were conducted to develop theoretical models that could help in understanding the nature of the backscattered ultrasonic signal (Angelsen, 1980; Mo and Cobbold, 1986, 1992; Twersky, 1987; Shung and Thieme, 1993; Bascom and Cobbold, 1995). The backscattered power, one of the parameters that can be extracted from the signal, was shown to be a function of the hematocrit, the size of the scatterers, and the frequency of the incident wave. These models also demonstrated the important role of the spatial arrangement of the scatterers in determining the ultrasonic backscattered power. Despite of the progress made in this field of research, there are still several aspects that need to be clarified, such as the behavior of the backscattered power at high frequencies (>40 MHz) or the effect of the spatial arrangement of the scatterers.

To better understand the scattering process by blood, simulation models were also developed. Routh et al. (1987)

modeled the RBCs by a set of identical, parallel slabs, randomly positioned. The slab thickness was kept constant, but the average distance between slabs was adjusted so as to model different hematocrits. The backscattered power as a function of the frequency and the hematocrit was studied. The results for this one-dimensional (1D) model suggested a square law dependence between the backscattered power and the frequency, and a maximum backscattered power at ~35% hematocrit. These results were in agreement with the 1D Rayleigh scattering theory, except for its prediction of an artifactual second peak near 90% hematocrit.

Following this study, another approach was used to model the reflection of ultrasound by a chain of randomly spaced elements, fixed at both ends (Gough et al., 1988). Routh et al. (1989) also studied the reflection by a chain of scatterers arranged in the steps of a 1D random walk, fixed at one end. In both studies, the power as a function of the hematocrit was evaluated, and the results were comparable to those obtained in their previous study (Routh et al., 1987). Mo et al. (1994) later studied the relationship between the backscattered power and the hematocrit by adapting the model of Routh et al. (1987). The simulation model was modified to allow random boundary conditions. The backscattered power increased at low hematocrits, peaked around 35% hematocrit, and decreased at higher hematocrits. The artifactual second peak at 90% hematocrit was not observed with this model, which is in agreement with the experimental results presented in the study.

However, it is known that the backscattered power from nonaggregating RBCs does not peak at 35% hematocrit and does not follow a second power frequency dependence. Instead, experimental results showed a peak of the backscattered power around 15% hematocrit (Shung, 1982;

Received for publication 8 February 1999 and in final form 20 July 1999.

Address reprint requests to Dr. Guy Cloutier, Laboratory of Biomedical Engineering, Institut de Recherches Cliniques de Montréal, 110 avenue des Pins Ouest, Montréal, QC H2W 1R7, Canada. Tel.: 514-987-5745; Fax: 514-987-5705; E-mail: cloutig@ircm.qc.ca.

© 1999 by the Biophysical Society

0006-3495/99/11/2387/13 \$2.00

Yuan and Shung, 1988b) and a fourth power frequency dependence when Rayleigh scattering conditions are satisfied (Shung et al., 1976; Yuan and Shung, 1988a). To overcome these limitations, Zhang et al. (1994) extended the 1D approach to a two-dimensional (2D) model. The highest hematocrit that could be modeled for this 2D simulation was 46%. The backscattered power as a function of the hematocrit peaked at 35% hematocrit in 1D and at 22% hematocrit in 2D. The validity of the Born approximation as well as the influence of the variation of the scatterer size and acoustical impedance were also studied. No results were presented on the frequency dependence of the backscattered power. Currently, neither 1D nor 2D simulation models can reproduce the experimental results obtained as a function of the hematocrit and frequency. Zhang et al. (1994) concluded that a 3D simulation model should provide better results.

In the present study, a system-based approach is proposed to model the backscattering of ultrasound by nonaggregating RBCs. It is based on an earlier model developed by Bamber and Dickinson (1980) for ultrasound image formation of living tissues and later expanded by Meunier and Bertrand (1995) to study tissue dynamics. This system-based model is adapted here to simulate the ultrasonic signal backscattered by blood. In this system-based model, the characteristics of the RBCs are defined in 3D, which should alleviate some limitations of the simulation models described previously. Furthermore, as will be shown later, the model explicitly considers the spatial arrangement of the scatterers, an important parameter affecting the backscattered signal. The choice of this model was governed by its flexibility in defining the transducer and tissue characteristics. The possibility of adapting the model to the study of moving RBCs was another motivation (Meunier and Bertrand, 1995).

The first part of this manuscript describes the main properties of the ultrasonic signal backscattered by blood and a summary of the different theoretical modeling approaches proposed in the literature. The system-based model is detailed in the second part of the manuscript. The model is used to study the effect of the spatial arrangement of the scatterers on the backscattered signal, and the hypothesis stating that the power of the backscattered signal is proportional to the variance of the local RBC concentration. More specifically, this simulation model was used to study the backscattered power as a function of the hematocrit, the volume of the scatterers, and the incident wave frequency. The Results and Discussion are presented in the last sections. In the last part of the Discussion, a new approach to modeling the spatial arrangement of the scatterers is proposed. This approach is based on the renewal point process theory.

THEORETICAL BACKGROUND

Scattering from one particle

An important parameter characterizing the ultrasonic signal backscattered by a single scatterer is the differential scat-

tering cross section (σ), which is the power scattered per solid angle per unit incident intensity (Shung and Thieme, 1993). Because RBCs are much smaller than the acoustical wavelength (for the range of frequencies usually used in medicine, 2–30 MHz), ultrasound scattering by nonaggregating RBCs follows the Rayleigh scattering theory (Rayleigh, 1945). This theory implies that the incident wave is scattered in all directions and that the scattering cross section is proportional to the fourth power of the incident wave frequency and to the square of the scatterer volume, a behavior that does not depend on the geometry of the scatterer (Rayleigh, 1945; Morse and Ingard, 1968). For weak scatterers, i.e., with density and compressibility that only differ slightly from the surrounding medium, and for arbitrary shape, the differential scattering cross section at an angle θ is given by (Shung and Thieme, 1993; Lucas and Twersky, 1987)

$$\sigma(\theta) = \frac{k^4 V_s^2}{16\pi^2} \left| \left(1 - \frac{\kappa_e}{\kappa_0} \right) - \left(1 - \frac{\rho_0}{\rho_e} \right) \cos(\theta) \right|^2, \quad (1)$$

where k is the wavenumber, V_s is the volume of the scatterer, ρ_0 and ρ_e are the densities (g/cm^3) of the surrounding medium and of the scatterer, respectively, and κ_0 and κ_e are their respective compressibilities (cm^2/dyne). The wavenumber is defined as $k = 2\pi/\lambda = 2\pi f/c$, where λ is the wavelength, f is the frequency of the propagating wave, and c is the speed of sound in the medium, which is equal to $(\kappa_0 \cdot \rho_0)^{-1/2}$ cm/s (Lucas and Twersky, 1987).

It is generally assumed that Rayleigh scattering occurs when $ka < \pi/10$, where a is the radius of the scatterer (Shung and Thieme, 1993). Beyond that limit, the behavior of the backscattered power by a single particle becomes dependent on the scatterer's geometry. For a scatterer radius much larger than the wavelength, exact solutions of the backscattered power exist for specific geometries such as a sphere (Morse and Ingard, 1968; Ishimaru, 1978). The characteristics of the power backscattered by a scatterer of arbitrary density and compressibility, whose radius is in the same range as the wavelength, still need to be studied (Kuo and Shung, 1994). The better understanding of ultrasound backscattering by blood in the non-Rayleigh region is relevant for ultrasonic imaging devices, operating at high frequencies, that are currently being developed to study microcirculation, for example (Turnbull et al., 1995; Christopher et al., 1997; Ferrara et al., 1996).

Scattering intensity from a random distribution of small particles

For a low volume concentration (hematocrit) of randomly positioned scatterers, the total backscattered power approximates the sum of echoes from all scatterers and is therefore proportional to the number of scatterers. However, for a dense suspension of scatterers, uncorrelated scatterer positions can no longer be assumed, even under nonaggregating conditions. Because of its finite size, a particle will prevent

others from occupying any position within a certain distance, and thus significant positioning correlation can exist. Under these conditions, the power of the backscattered signal is a function of the scatterer spatial arrangement and is not simply proportional to the number of scatterers.

The backscattering coefficient (BSC) is, by definition, the average backscattered power per steradian from a unit volume of blood, insonated by a plane wave of unit intensity (Shung and Thieme, 1993). In Mo and Cobbold (1992), the BSC was given by

$$\text{BSC} = \sigma_{\text{bs}}(H/V)W, \quad (2)$$

where σ_{bs} is the differential scattering cross section defined in Eq. 1 for $\theta = 180^\circ$, H is the hematocrit, V is the average volume of the scatterers, and W is the packing factor. The packing factor is a measure of the orderliness in the spatial arrangement of the particles. It expresses the acoustic interference between all echoes. It was derived from the following statistical mechanics structure factor for symmetrical pair-distributed functions (Twersky, 1975, 1987):

$$W(k, (\hat{r}_i - \hat{r}_o)) = 1 + \rho \int [g(R_p) - 1] e^{ik(\hat{r}_i - \hat{r}_o) \cdot R_p} dR, \quad (3)$$

where k is the wavenumber; \hat{r}_i and \hat{r}_o are, respectively, unit vectors in the direction of the incident wave and in the direction of observation; ρ is the density of particles, $[g(R_p) - 1]$ is the total correlation function, where $g(R_p)$ is the radial distribution function; R_p is the separation of pairs; j is $\sqrt{-1}$; and $\int dR$ is the corresponding volume integral (i.e., $\iiint dx dy dz$). This expression (Eq. 3) was obtained by considering an incident plane wave. The radial distribution function, $g(R_p)$, represents the probability of finding two particles separated by a distance R_p in the volume.

The packing factor is the low-frequency limit of this structure factor (i.e. $k \rightarrow 0$) and is thus given by (Twersky, 1975, 1987)

$$W = 1 + \rho \int [g(R_p) - 1] dR. \quad (4)$$

The packing factor can also be expressed as a function of the variance of the local scatterer concentration (Twersky, 1987), i.e.,

$$W = (1/\bar{n}) \overline{\text{var}(n)}, \quad (5)$$

where \bar{n} is the average number of scatterers within all elemental blood volumes (voxels), and $\overline{\text{var}(n)}$ is the variance in the mean number of scatterers within each elemental voxel averaged over space and time. (In the definition of a voxel, the thickness of the volume parallel to the propagation plane wave is less than $\lambda/10$.) The Percus-Yevick approximation model describing the pair-correlation for identical, randomly positioned spherical particles can be used to express W as a function of the hematocrit (Twersky,

1975):

$$W = \frac{(1 - H)^4}{(1 + 2H)^2}. \quad (6)$$

This factor approaches 1 at a very low hematocrit because the positions of RBCs are then almost perfectly uncorrelated. It decreases as the hematocrit increases, until it reaches 0 at 100% hematocrit.

The average number of scatterers per voxel is $\bar{n} = H \cdot \Omega_e/V = \rho \cdot \Omega_e$, where Ω_e represents the voxel size and ρ is defined in Eq. 3. Hence using Eqs. 5 and 2, the backscattering coefficient can also be expressed as

$$\text{BSC} = \sigma_{\text{bs}} \overline{\text{var}(n)} / \Omega_e. \quad (7)$$

This last equation shows that the backscattered power should be proportional to the variance of the local scatterer concentration. Interestingly, Eq. 7 indicates that a null variance situation, i.e., where the number of scatterers within each voxel is constant, should lead to a backscattered power of 0, independently of the hematocrit. This phenomenon is called crystallographic scattering, and it can be explained by a perfect destructive interference pattern (Shung and Thieme, 1993).

Several studies compared the theoretical BSC as a function of the hematocrit (Eq. 2) with experimental observations (Shung, 1982; Shung et al., 1984; Lucas and Twersky, 1987; Berger et al., 1991). With the packing factor given by Eq. 6, it was found that the experimental and theoretical curves did not match perfectly because the packing of RBCs certainly differs from that of rigid spheres. To overcome this problem, a new packing factor was introduced to take into consideration the effect of the shape of the scatterers, the nature of the flow, and the polydispersity in the size of the scatterers. The equation describing the new packing factor is (Berger et al., 1991)

$$W = \frac{(1 - H)^2}{[1 + (d_1 - 1)H]^2} \times \left\{ (1 - H)^2 + (1 - H)H \frac{4d_1d_2}{1 + 5d_2} + \frac{H^2d_1^2d_2}{1 + 4d_2} \right\}, \quad (8)$$

where H is the hematocrit, d_1 considers the shape and correlation among scatterers, and d_2 represents the variance in the particle size. For a suspension of identical rigid spheres, the parameters d_1 and d_2 are, respectively, 3 and 0, and Eq. 8 becomes equivalent to Eq. 6.

METHODS

Simulation model

The system-based model uses the Born approximation, which implies that the scattered echoes are weak compared to the incident signal. It is then possible to assume that the impulse response of the system is space-invariant within a small region (Meunier and Bertrand, 1995). The Born

approximation also implies that it is possible to use the principle of superposition to represent the wave scattered by a collection of particles by adding their respective contribution. The radio frequency (RF) signal received by the ultrasound transducer translated in the (x, z) plane can be modeled as

$$\text{RF}_{3d}(x, y, z) = \frac{\partial^2}{\partial y^2} T_{3d}(x, y, z) \otimes Z_{3d}(x, y, z), \quad (9)$$

where $T_{3d}(x, y, z)$ represents the system three-dimensional (3D) point spread function (PSF), and $Z_{3d}(x, y, z)$ describes the acoustical impedance of the scatterers. In Eq. 9, x and z are, respectively, along the lateral and elevation directions, and y is in the direction of propagation of the ultrasonic wave. The RF signal in Eq. 9 is determined by the transducer transfer function, $T_{3d}(x, y, z)$, convoluted by the fluctuations of the tissue impedance, i.e., $(\partial^2/\partial y^2) Z_{3d}(x, y, z)$. It is assumed that the incident acoustic wave is not modified by the small inhomogeneities encountered in the volume. Because multiple reflections are neglected, the backscattered RF signal is thus the sum of the acoustic responses from each point in the sample volume. The complete mathematical development leading to this equation can be found in Meunier and Bertrand (1995).

The RF signal required for one-dimensional analysis corresponds to one line of the whole 3D RF signal, and it can be obtained by evaluating Eq. 9 at $z = 0$ and $x = 0$. More specifically,

$$\text{RF}(y) = \text{RF}_{3d}(0, y, 0)$$

$$= \frac{\partial^2}{\partial y^2} \iiint Z_{3d}(\mu, \nu, \omega) T_{3d}(-\mu, y - \nu, -\omega) d\mu d\nu d\omega. \quad (10)$$

Assuming a separable PSF, i.e., $T_{3d}(x, y, z) = T_x(x)T_y(y)T_z(z)$, $\text{RF}(y)$ becomes

$$\text{RF}(y) = \frac{\partial^2}{\partial y^2} T_y(y) \otimes Z(y), \quad (11)$$

where $Z(y)$ is the projection of the 3D acoustical impedance function (Z_{3d}), weighted by the PSF over the x - z plane, i.e.,

$$Z(y) = \iint Z_{3d}(x, y, z) T_x(-x) T_z(-z) dx dz. \quad (12)$$

The impedance function Z_{3d} is determined by the fluctuations in density and compressibility of the medium. It can be made to represent a homogeneous medium of mean impedance Z_0 that embeds the scatterers with acoustical impedance $Z_0 + \Delta Z$ (Meunier and Bertrand, 1995). This mean impedance Z_0 can be ignored because of the second derivative operator of the model. Furthermore, the impedance function can be simplified by assuming that all scatterers are identical in shape and echogenicity. It is then possible to represent the RBCs by a single scatterer prototype $C_{3d}(x, y, z)$ that is repeated at each cell position (x_n, y_n, z_n) . The 3D impedance function can then be written as

$$Z_{3d}(x, y, z) = \sum_{n=1}^M Z_n(x, y, z) \\ = \sum_{n=1}^M C_{3d}(x - x_n, y - y_n, z - z_n), \quad (13)$$

where M is the number of scatterers. Equation 13 is equivalent to

$$Z_{3d}(x, y, z) = C_{3d}(x, y, z) \otimes \sum_{n=1}^M \delta(x - x_n, y - y_n, z - z_n) \\ = C_{3d}(x, y, z) \otimes N(x, y, z), \quad (14)$$

where $N(x, y, z)$ is called the microscopic density distribution. This function is nonzero at the center position of every RBC. The size and echogenicity of the RBCs are considered by the convolution of $N(x, y, z)$ with $C_{3d}(x, y, z)$. It can be shown that the Fourier transform of the microscopic density distribution is proportional to the structure factor described before in Eq. 3. A system-based interpretation of the structure factor is given in the Appendix for the special case of ultrasound backscattering.

Using previous definitions and assuming that the PSF is constant over the dimension of a scatterer in the x - z plane, the impedance function defined in Eq. 12 can be written in terms of a convolution:

$$Z(y) = C(y) \otimes N(y), \quad (15)$$

where

$$C(y) = \iint C_{3d}(x, y, z) dx dz, \quad (16)$$

and $N(y)$ is defined by

$$N(y) = \sum_{n=1}^M T_x(-x_n) T_z(-z_n) \delta(y - y_n). \quad (17)$$

Consequently, from Eqs. 11 and 15, the RF signal received by the transducer can be written as

$$\text{RF}(y) = \frac{\partial^2}{\partial y^2} T_y(y) \otimes C(y) \otimes N(y). \quad (18)$$

The function $N(y)$ conveys information about the spatial arrangement of the scatterers and is, by definition, nonzero at every scatterer location. It is a projection on the y axis of each scatterer's echogenicity weighted by the magnitude of the PSF at the scatterer's position. A simpler interpretation of $N(y)$ is possible when $T_x(x)$ and $T_z(z)$ are constant over the width and thickness of the sample volume. In this case, $N(y)dy$ represents the number of scatterers contained in the corresponding slice dy of the sample volume. In summary, the ultrasonic signal backscattered by blood can be computed by the convolution of the transducer transfer function (T_y) with the scatterer prototype (C) and the function N that represents the density distribution of the scatterers.

Implementation for computer simulations

To compute the ultrasonic signal backscattered by RBCs, the transducer function, the scatterer prototype, and the spatial distribution of the scatterers need to be defined.

Definition of the PSF (T)

As used by Meunier and Bertrand (1995), the PSF representing the system response is a 3D Gaussian envelope modulated by a cosine function:

$$T_{3d}(x, y, z) = \exp\left[-\frac{1}{2}\left(\frac{x^2}{\psi_x^2} + \frac{y^2}{\psi_y^2} + \frac{z^2}{\psi_z^2}\right)\right] \cos\left(\frac{4\pi fy}{c}\right). \quad (19)$$

In the above equation, ψ_x , ψ_y , and ψ_z are the standard deviations of the 3D Gaussian function representing the beamwidth, the transmitted pulse

length, and the beam thickness, respectively. The parameters $2f/c$, in Eq. 19, represent the transducer spatial frequency, where f is the ultrasonic frequency and c is the speed of sound. In this paper, the PSF is modeled with $\psi_x = 0.43$ mm, $\psi_y = 0.21$ mm, and $\psi_z = 0.85$ mm. It is easy to show that the hypothesis of separability used above is valid for this PSF definition. The function $T_y(y)$ used for the 1D analysis corresponds to $T_{3d}(0, y, 0)$.

Scatterer prototype (C)

In our simulations, the scatterer prototype was approximated by a sphere. The function $C(y)$, which is the projection of the scatterer on the y axis, can be written in this case as

$$C(y) = \pi(a^2 - y^2), \quad (20)$$

where the parameter a corresponds to the radius of the sphere. Human RBCs were approximated by spherical scatterers having a volume of $87 \mu\text{m}^3$ (Shung and Thieme, 1993), which corresponds to a radius of $2.75 \mu\text{m}$ (diameter of $5.5 \mu\text{m}$). For simulations performed to study the effect of the scatterer volume on the backscattered power, the radius a was changed accordingly.

Simulations were also performed using the scatterer geometry defined previously by Meunier and Bertrand (1995). In that study, scatterers were modeled as 3D Gaussians. In the present study, this scatterer geometry was used to assess the effect of the shape of the scatterer on the backscattered power as a function of the frequency. The backscattered power is known to be independent of the shape of the scatterer for Rayleigh scattering, but this property may not be valid for non-Rayleigh scatterers. In 1D, the Gaussian scatterer prototype can be expressed by

$$C(y) = 2\pi\sqrt{\sigma_x^2 \cdot \sigma_z^2} \exp\left(\frac{-1}{2} \cdot \frac{y^2}{\sigma_y^2}\right), \quad (21)$$

where σ_x , σ_y , and σ_z are the standard deviations corresponding to the scatterer size in the x , y , and z planes. The standard deviations of the scatterer prototype were set to the radius of the sphere defined in Eq. 20 ($\sigma_x = \sigma_y = \sigma_z = 2.75 \mu\text{m}$).

Spatial distribution (N)

One original aspect of this simulation model is the possibility of incorporating the effect of the 3D spatial distribution of the scatterers on the BSC. Recall that the function $N(y)$ can be interpreted as the number of scatterers contained in each slice y_n of thickness dy in the sample volume. If the number of scatterers in a slice of thickness dy is large, then for randomly positioned scatterers, the central limit theorem predicts that $N(y)$ is the outcome of a normal stochastic process (Papoulis, 1991). Thus, the first-order statistics of $N(y)$ requires specifying its mean and variance, which, in our case, are given by $\bar{n} = H \cdot \Omega_c/V$ and $\overline{\text{var}(n)} = \bar{n}W$, respectively. The two different definitions of the packing factor given by Eqs. 6 and 8 were used in the definition of the function N .

RF signal

As mentioned before, the ultrasound signal is computed by the convolution of $(\partial^2/\partial y^2) T_y(y)$, $C(y)$, and $N(y)$. The convolution of these functions in the time domain is equivalent to a simple product of their Fourier transforms in the spectral domain. The spectra of those functions, as defined previously, are presented in Fig. 1. The spectrum of the second derivative of the PSF is shown in Fig. 1 a, and the spectra of the two different scatterer geometries, i.e., the sphere and the Gaussian, are shown in Fig. 1 b. The function representing the spectrum of the spatial arrangement of the scatterers (N) is illustrated in Fig. 1 c. The spectrum is that of a white noise whose expected power level is proportional to the variance of the number of scatterers within each elemental voxel ($\overline{\text{var}(n)} = \Omega_c(H/V)W$), when

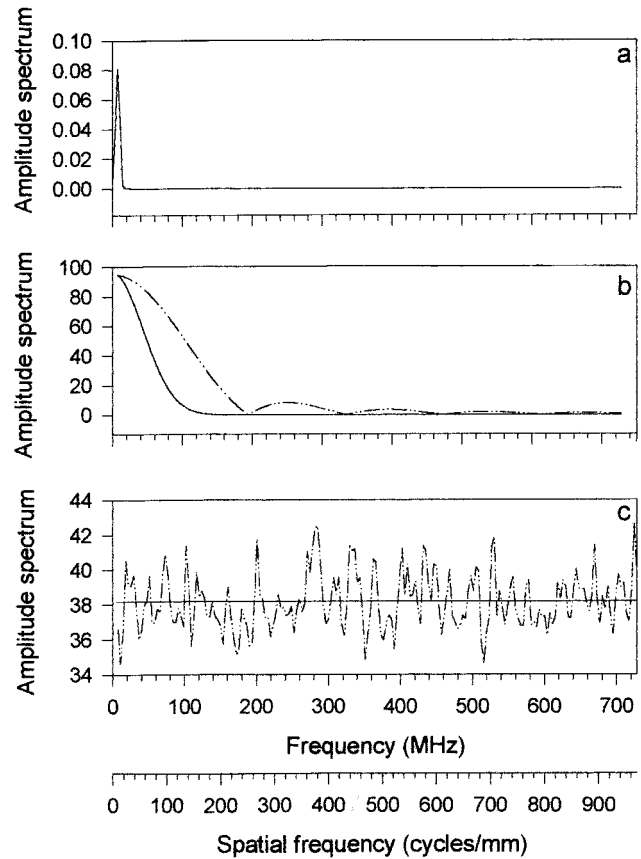


FIGURE 1 (a) Amplitude spectrum of the second derivative of the PSF $((\partial^2/\partial y^2)T_y(y))$. $T_y(y)$ is computed from Eq. 19, with the transducer frequency $f = 7.5$ MHz. (b) Amplitude spectrum of the scatterer prototype $C(y)$ for $a = 2.75 \mu\text{m}$. \cdots , The sphere prototype (Eq. 20); — , the Gaussian prototype (Eq. 21). The maximum value of the first function was normalized with respect to that of the second one. (c) Amplitude spectrum of the distribution $N(y)$ at 40% hematocrit, computed using the packing factor. \cdots , The simulation results averaged over 10 simulations. — , The theoretical spectrum, the amplitude of which is proportional to the variance in the mean number of cells. The spatial frequency in cycles/mm is also indicated on the x axis.

averaged over several realizations of the same statistical process. The theoretical power spectrum of the function $N(y)$ is constant over all frequencies, for the packing factor definitions given by Eq. 6 or 8. As shown later in the Discussion, the microscopic density distribution may be more accurately modeled as a function of the frequency by using the point process theory.

As shown previously in Eq. 2, theoretical models suggest that the backscattered power is equal to $\sigma_{bs} (H/V)W$. The backscattering cross section σ_{bs} is considered by the second derivative of the transducer function $(\partial^2/\partial y^2) T_y(y)$ operating on the cell prototype function (C). The spatial distribution of the scatterers (N) reflects the acoustic interference associated with the presence of many scatterers and leads to the coefficient $(H/V)W$ of the theoretical model.

Comparison of the simulations with theory and experimental results

The simulations were compared to the theoretical BSC given by Eqs. 1 and 2 and to experimental results obtained by Shung and collaborators (Shung et al., 1984; Yuan and Shung, 1988a; Shung et al., 1993). The surrounding medium considered in this work was an isotonic saline solution because

RBCs washed and suspended in saline do not form aggregates. The following values were used to compute the theoretical backscattering cross section defined by Eq. 1 ($\theta = 180^\circ$): for human red cells, $\kappa_c = 34.1 \times 10^{-12} \text{ cm}^2/\text{dyne}$ and $\rho_c = 1.092 \text{ g/cm}^3$; and for the isotonic saline solution, $\kappa_0 = 44.3 \times 10^{-12} \text{ cm}^2/\text{dyne}$ and $\rho_0 = 1.005 \text{ g/cm}^3$.

The size of the sample volume in the direction of propagation y was 2.048 mm, and the resolution within the 3D volume was $0.5 \mu\text{m}$, corresponding to a sampling frequency of 1.57 GHz. (The sampling frequency is obtained by dividing $c/2$ by the spatial resolution of $0.5 \mu\text{m}$.) This resolution was chosen to prevent significant aliasing for the RBC prototype (C) and the PSF (T_y). This small resolution allows the modeling of each RBC with many "scattering points." The tissue is thus represented by a large number of points, either within or outside each RBC. As mentioned before, the surrounding medium has an acoustical impedance Z_0 , while all RBCs have the same impedance, characterized by the convolution of the scatterer prototype function (C) with the position matrix (N). The voxel size used for projecting the 3D volume into 1D was determined in the x - z plane by the dimensions of the PSF. The width and thickness of the PSF were estimated by twice the FWHM (full width half-maximum), which is ~ 2.35 multiplied by the standard deviation (ψ) (Meunier and Bertrand, 1995). Using the standard deviations defined previously, the width of the voxel thus corresponded to 2 mm and the thickness to 4 mm. In the simulations, 4096 voxels were used ($2048 \mu\text{m}/0.5 \mu\text{m}$), and the dimension of the voxel (Ω_c) was $4 \times 10^{-3} \text{ mm}^3$ ($2 \text{ mm} \times 4 \text{ mm} \times 0.5 \mu\text{m}$).

All simulations were performed with Matlab 4.2 (The MathWorks Inc., Natick, MA). The backscattered power of the simulated signal $\text{RF}(y)$ was obtained by computing the mean value of the square of the amplitude of this signal. All simulations presented in the following section were computed 100 times for statistical averaging. All results were expressed in $\text{cm}^{-1}\text{steradian}^{-1}$ and were normalized with respect to the theoretical values obtained from Eq. 2. The normalization constant was computed by doing a linear regression of the backscattered powers over the range of hematocrits, frequencies, and volumes considered (see Figs. 2–7).

RESULTS

A spherical scatterer prototype $C(y)$ was used in all simulations, except when specified. Fig. 2 shows the relationship between the BSC and the hematocrit for human RBCs at 7.5 MHz. The simulation results (*circles*) are presented along with the theoretical BSC curve (*solid line*) obtained from Eq. 2, and experimental results obtained from a stationary erythrocyte suspension (*triangles*) (Shung et al., 1984). The packing factor used for the theoretical curve and the simulations was evaluated according to Eq. 6. As seen in this figure, there is a good agreement between the simulation and theoretical results. But, as also shown by Shung et al. (1984) and Lucas and Twersky (1987) for the theoretical data, neither of these results perfectly match the experimental data. The largest discrepancies are observed around the peak of the BSC curve and at high hematocrit values. The maximum power of the simulated and theoretical curves is observed near 13% hematocrit, while the peak of the experimental data occurs at 16% hematocrit.

As mentioned previously, the packing factor defined by Eq. 6 was derived for identical spheres. Equation 8 was proposed to better reproduce experimental results obtained for RBCs. Simulations were performed using this definition of the packing factor, with $d_1 = 1.723$ and $d_2 = 0$. The results obtained for these simulations are presented in Fig. 3. The maximum backscattering occurs at 16% hematocrit for all types of data, and a better agreement between the

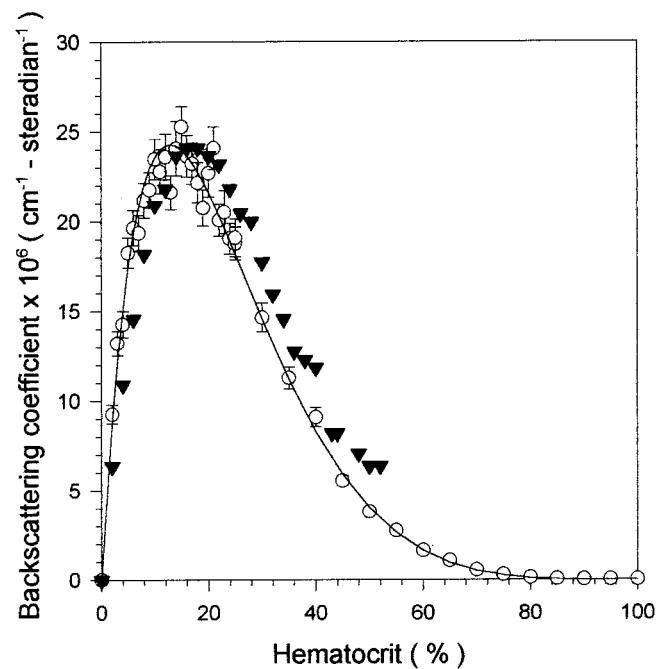


FIGURE 2 Backscattering coefficient as a function of the hematocrit at 7.5 MHz. \circ , Simulation results, which are expressed in terms of mean \pm one standard error ($n = 100$ simulations). —, The theoretical curve, computed from Eqs. 1 and 2. The packing factor of Eq. 6 was used for the simulations and theoretical results. \blacktriangledown , Experimental results reproduced from Shung et al. (1984).

theoretical, simulation, and experimental results is observed at high hematocrits. It is important to note that these values of d_1 and d_2 are specific for these scatterer and static flow characteristics. These values would be different under laminar or turbulent flow conditions and in the presence of RBC aggregation, because these conditions affect the spatial arrangement of the scatterers.

All other simulations presented in the Results were done with the packing factor expressed by Eq. 6. These simulations were performed to study the properties of the backscattered signal in relation to the volume of the scatterers and the frequency. Fig. 4 shows the BSC as a function of the frequency of the propagating wave. The full line represents the fourth-power dependence predicted by the theory (Eqs. 1, 2, and 6). The triangles correspond to experimental measurements obtained by Yuan and Shung (1988a) at a hematocrit of 44%, using bovine whole blood, which is known to form very few aggregates (Weng et al., 1996). The circles and diamonds correspond to the simulation results. The circles represent simulations performed with a spherical scatterer prototype, and the diamonds represent those performed with the Gaussian scatterer prototype. These simulations were done at 40% hematocrit for frequencies ranging from 2–500 MHz, the latter being well beyond frequencies used for cardiovascular applications. Both curves are in good agreement with the theoretical and experimental data at low frequencies. But it can be seen in Fig. 4 that the behaviors of the two simulated BSC curves differ at high ka

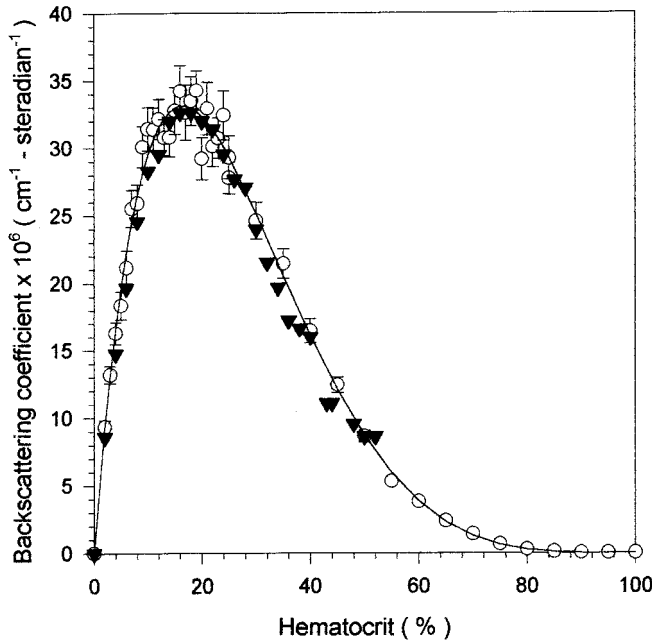


FIGURE 3 Backscattering coefficient as a function of the hematocrit at 7.5 MHz. \circ , Simulation results, which are expressed in terms of mean \pm one standard error ($n = 100$ simulations). —, The theoretical curve, computed from Eqs. 1 and 2. The packing factor of Eq. 8 was used for the simulations and theoretical results. \blacktriangledown , Experimental results reproduced from Shung et al. (1984). Because all results were normalized with respect to the theoretical curve, the scaling of the y axis on this figure and that in Fig. 2 are different.

values. For the Gaussian scatterers, the backscattered power decreases in the non-Rayleigh region, while for the spherical scatterers, the backscattered power rather oscillates around a constant value. Neither of the two curves follows the theoretical prediction for Rayleigh scattering at high frequencies (above ~ 40 MHz).

The backscattered power as a function of the volume of the scatterers was also studied for a range of volume well beyond that of normal human RBCs. These simulations were performed to better understand the fundamental mechanisms of ultrasound backscattering. Figs. 5 and 6 show the results obtained for scatterer volumes ranging between $4.2 \mu\text{m}^3$ and $220 \mu\text{m}^3$, at a fixed scatterer number density ($\bar{n}/\Omega_e = H/V = \text{a constant}$). The results of Fig. 5 were obtained for a cell concentration of $6 \times 10^5 \text{ cells/mm}^3$, and Fig. 6 corresponds to a cell concentration of $40 \times 10^5 \text{ cells/mm}^3$. The circles correspond to the simulations, and the triangles (Fig. 5) correspond to experimental results obtained by Shung et al. (1993) for porcine, bovine, and lamb RBCs. The full line represents the theoretical volume square relationship multiplied by the packing factor (V^2W). This relationship is obtained from Eq. 2 ($\text{BSC} = \sigma_{\text{bs}} (H/V)W$, where the ratio H/V is a constant for a fixed number density of RBCs, and σ_{bs} is proportional to V^2). The hematocrit scale corresponding to the simulation conditions is also indicated on the x axis. In both figures, a good agreement was obtained between the theoretical curves and the simu-

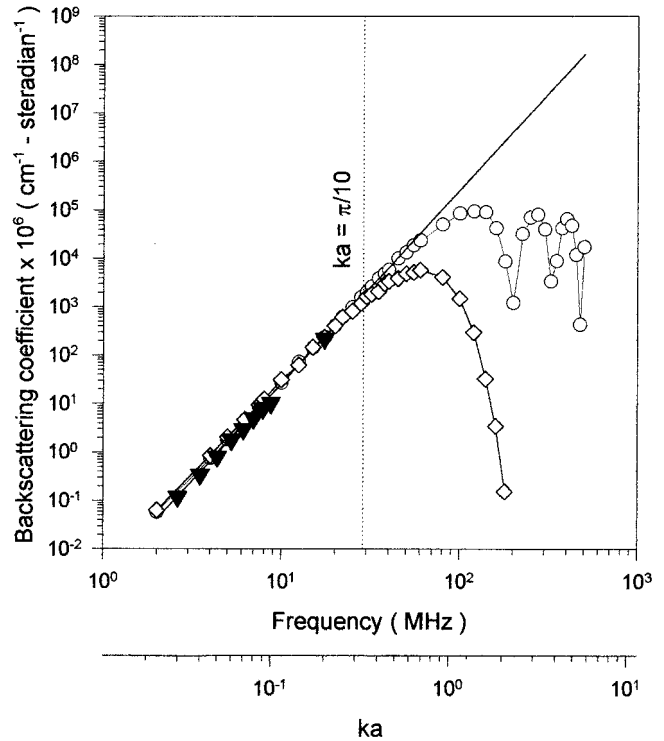


FIGURE 4 Backscattering coefficient as a function of the frequency at 40% hematocrit. \circ , Simulation results using a spherical scatterer prototype; \diamond , simulation results using a Gaussian scatterer prototype. Both are expressed in terms of mean \pm one standard error ($n = 100$ simulations). —, The theoretical fourth-power frequency dependence. \blacktriangledown , Experimental results reproduced from Yuan and Shung (1988a). The normalization constant of the simulation and experimental results was computed for frequencies between 2 and 20 MHz. The parameters ka corresponding to the frequency scale are also indicated on the x axis, where k is the wavenumber and a is the radius of the scatterers.

lation results. In Fig. 5, the results also agreed well with experimental data.

Finally, a last series of simulations was done to better determine the relationship between the backscattered power and the size of the scatterers at a constant hematocrit (volume concentration) of 40%, which implies a constant value of the packing factor for nonaggregating RBCs. The simulation results are presented in Fig. 7. The full line obtained from Eqs. 1 and 2 shows a linear dependence between the backscattering coefficient and the volume of the scatterers ($\text{BSC} = \sigma_{\text{bs}} (H/V)W$, where H and W are constant, and σ_{bs} is proportional to V^2). The simulation results are in good agreement with the theory for the range of volumes considered. The cell concentration corresponding to the range of volumes is also given on the x axis.

DISCUSSION

Analysis of the results

The results, which are in very good agreement with the theory and experimental data, confirm the validity of this model for simulation of the ultrasonic signal backscattered

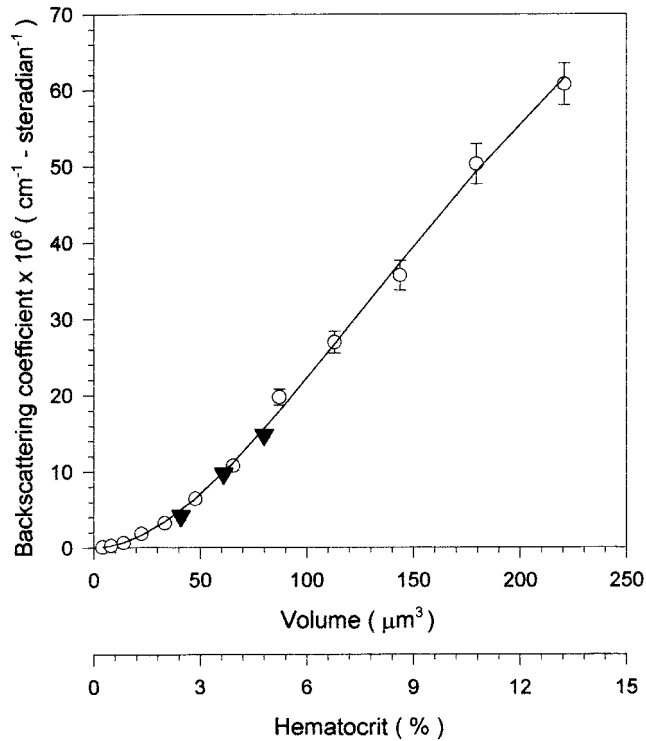


FIGURE 5 Backscattering coefficient at 7.5 MHz as a function of the volume of the scatterers for a constant scatterer concentration of 6×10^5 cells/mm³. \circ , Simulation results, which are expressed in terms of mean \pm one standard error ($n = 100$ simulations). —, The theoretical volume square relationship multiplied by the packing factor. \blacktriangledown , Experimental results reproduced from Shung et al. (1993). The hematocrits corresponding to the volume scale are also indicated on the x axis.

by RBCs. The system-based approach provided more accurate modeling than previous simulation models (Routh et al., 1987, 1989; Gough et al., 1988; Mo et al., 1994; Zhang et al., 1994). One of the reasons why our results provided a better agreement with the experimental observations is that the geometry of the scatterers was defined in 3D (spherical or Gaussian scatterers), while in previous 1D and 2D simulation models, slabs (Routh et al., 1987, 1989; Gough et al., 1988; Mo et al., 1994; Zhang et al., 1994) and cylinders (Zhang et al., 1994) were used. Moreover, the spatial arrangement was defined to represent the characteristics of scatterers suspended in a 3D volume, by using the appropriate packing factor.

As mentioned before, theoretical modeling showed the importance of the spatial arrangement of the scatterers on the backscattered power. In the present simulation model, the spatial distribution of the scatterers was modeled by considering the packing factor theory (see Figs. 2 and 3). More specifically, the backscattered power was shown to be proportional to the local variance of the scatterers ($\text{var}(n) = \bar{n}W$). It is known from the literature that the spatial arrangement of the scatterers depends on the scatterer and flow characteristics. The flexibility of the system-based model allows the properties of the backscattered signal to be modeled for different characteristics of the flow and scatterers,

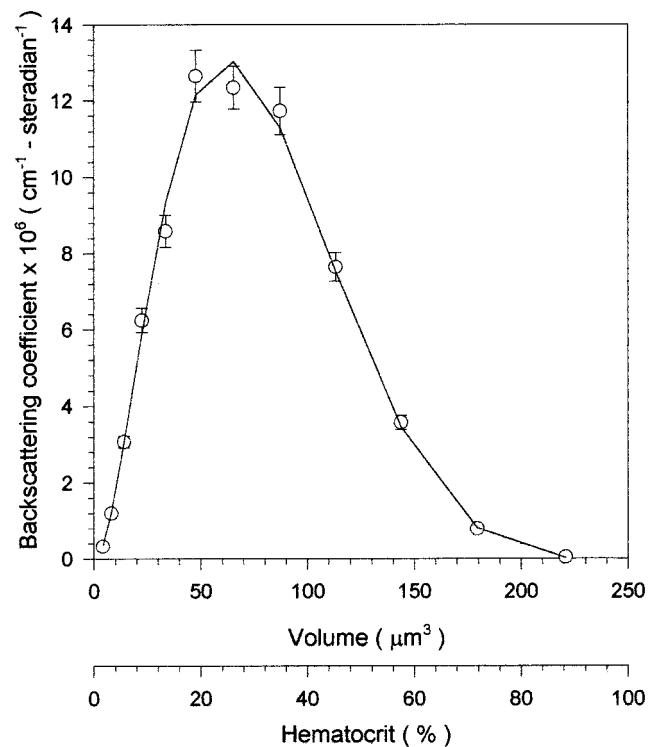


FIGURE 6 Backscattering coefficient at 7.5 MHz as a function of the volume of the scatterers for a constant scatterer concentration of 40×10^5 cells/mm³. \circ , Simulation results, which are expressed in terms of mean \pm one standard error ($n = 100$ simulations). —, The theoretical volume square relationship multiplied by the packing factor. The hematocrits corresponding to the volume scale are also indicated on the x axis.

by simply using the appropriate packing factor. However, the definition of the packing factor as a function of these characteristics needs to be further investigated.

The theoretical model used to compare our simulation results (Eqs. 1 and 2) is based on the Rayleigh scattering theory. The results of Fig. 4 are in agreement with this theory, which suggests a fourth-power dependence at least up to 30 MHz (Shung et al., 1993; Kuo and Shung, 1994) (the limit of Rayleigh scattering is usually approximated by $ka = \pi/10$ (Ishimaru, 1978; Shung and Thieme, 1993)). For $ka < \pi/10$, the simulations provided a 3.9 power dependence. Very interestingly, the simulation results of Fig. 4 obtained for spherical scatterers are in agreement with theoretical results obtained using the T-matrix method for spherical scatterers and biconcave scatterers mimicking RBCs (Kuo and Shung, 1994) at high frequencies. The different behavior obtained for the two scatterer prototypes can be explained by the fact that the Gaussian geometry is not limited in space, as opposed to the spherical geometry. The discontinuity at the sphere boundary produces a window effect that creates oscillations in the spectrum of the scatterer prototype at high frequencies, as shown in Fig. 1 *b*. The behavior of the backscattered power at high frequencies is thus mostly affected by the shape of the cell, as opposed to Rayleigh scattering, which is independent of the geometry of the scatterer.

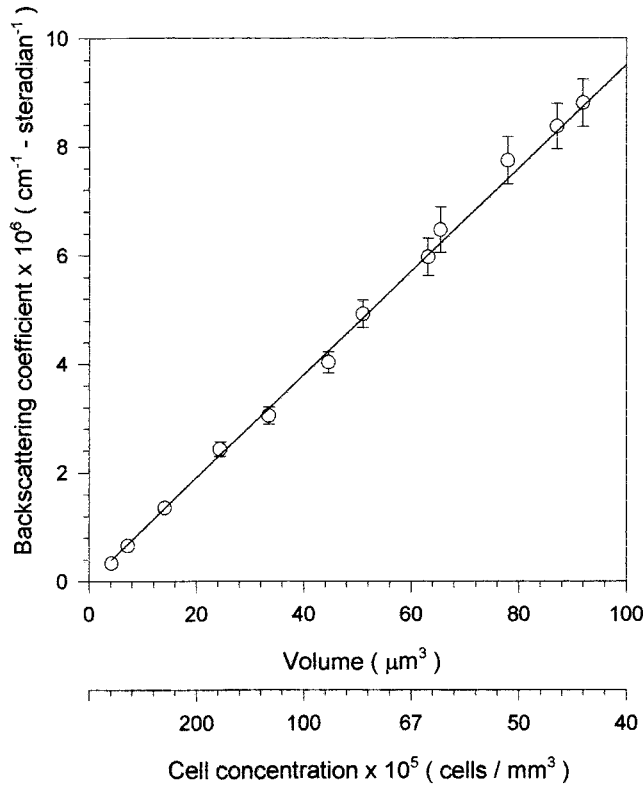


FIGURE 7 Backscattering coefficient at 7.5 MHz as a function of the scatterer volume, for a constant hematocrit of 40%. \circ , Simulation results, which are expressed in terms of mean \pm one standard error ($n = 100$ simulations). —, The theoretical linear volume relationship. The cell concentration corresponding to the range of volumes considered is also given on the x axis.

The experimental results presented in Fig. 5 were obtained by Shung et al. (1993) at a cell concentration of 6×10^5 cells/mm³, scatterer volumes up to $90 \mu\text{m}^3$ (maximum hematocrit = 5.5%), and an ultrasound frequency of 7.5 MHz. From these results, the BSC was found to be proportional to the square of the volume of the scatterers, which is in agreement with the theory for this low scatterer density. For instance, the packing factor of Eq. 6 is higher than 0.65 for hematocrits below 5.5%, which provided results close to the volume square relationship ($W \approx 1$, so the BSC is proportional to V^2 for a constant number density of scatterers). However, an increase in the volume of a fixed number of scatterers also results in an increase in the hematocrit, which affects the value of the packing factor. Even if the relationship between the BSC and the volume of the scatterers can be predicted from the theoretical equations, the literature is not clear on this topic (Shung et al., 1993). So, it should be made clear that the relationship between the BSC and the volume of the scatterers, for Rayleigh scattering, is V^2W at a fixed number density of scatterers. As shown in Fig. 6, the influence of the packing factor dominates over that of the volume square relationship at hematocrits higher than $\sim 22\%$. This effect is very important at high hematocrit values and leads to a decrease in the back-

scattering coefficient. The last simulations presented in Fig. 7 were done for different scatterer volumes at a constant hematocrit. In this case, the BSC is not affected by the packing factor, and it is linearly related to the volume of the scatterers.

A new approach to modeling the variance in the spatial arrangement of the scatterers

The results presented in this article were all obtained using the packing factor of Eq. 6 or 8 to model the variance in the spatial arrangement of the scatterers ($\text{var}(n) = \bar{n}W = \Omega_e (H/V)W$). We introduce here a new approach, inspired by the renewal process theory (Papoulis, 1991), to model the function $N(y)$. This approach was not used in the simulations presented in this article because it is currently being developed in 1D only. Despite this fact, interesting observations can be made at this point, as presented below.

The positions of a high density of scatterers are not completely random because of their finite size. For instance, two cells cannot occupy the same space. This phenomenon can be modeled by a particular point process, where the output is a series of pulses randomly positioned. In the case of scattering by RBCs, an event (pulse) represents a point at the cell location. The sequence of random intervals describing the distance between two adjacent pulses is called a renewal process (Papoulis, 1991). The distance between two pulses of a renewal point process is often represented by a random variable with an exponential probability density distribution. For cells of finite size, there is a null probability that two pulses are closer than the diameter of the cell, i.e., $2a$. The probability density that another cell is present at a distance τ can be expressed by the exponential density function,

$$f(\tau) = 0, \quad \tau < 2a$$

$$f(\tau) = \frac{1}{\mu} \exp(-(\tau - 2a)/\mu), \quad \tau > 2a, \quad (22)$$

where μ is the mean of the density distribution, and $\mu + 2a$ is the mean distance between two pulses. The Fourier transform of this density distribution is expressed by

$$F(j\omega) = \frac{\exp(-2j\omega a)}{1 + j\omega\mu}. \quad (23)$$

The power spectral density of the point process can be shown to be equal to (Shweddyk et al., 1977)

$$\Phi(j\omega) = \alpha \left(1 + 2 \text{Re} \left(\frac{F(j\omega)}{1 - F(j\omega)} \right) \right), \quad (24)$$

where α represents the average pulse density that is equal to $1/(2a + \mu)$. This equation can also be written as $\Phi(j\omega) =$

$\alpha[1 + \Psi(j\omega)]$, where

$$\Psi(j\omega) = 2 \operatorname{Re} \left\{ \frac{F(j\omega)}{1 - F(j\omega)} \right\} \\ = \frac{2(\cos(2\omega a) - \omega\mu \sin(2\omega a) - 1)}{2 + \omega^2\mu^2 - 2\cos(2\omega a) + 2\omega\mu \sin(2\omega a)}. \quad (25)$$

In 1D, the hematocrit is equivalent to the ratio of the cell diameter to the average distance between two cells (center position to center position), i.e., $H = 2a/(2a + \mu)$. For $2a = 5.5 \mu\text{m}$ and $H = 10\%$, 40% , and 70% , the power spectral density $\Phi(j\omega)$ is shown in Fig. 8. It can be seen that at 10% hematocrit, the power spectrum is almost constant over all frequencies. On the other hand, at 40% and 70% hematocrits, important oscillations can be observed with a dominant peak located at ~ 100 MHz. At 70% hematocrit, the oscillations of the power spectrum are higher, but the low-frequency limit is lower than that observed at 40% and 10% hematocrits. Unlike the power spectrum of $N(y)$ shown in Fig. 1 *c*, which does not depend on the frequency, the renewal process theory suggests that there is a frequency dependence in the range of frequencies considered.

As shown below, even if the power spectra obtained from the two described approaches seem different (Figs. 1 *c* and 8), their low-frequency limits are equivalent (the mean amplitude in Fig. 1 *c* is slightly different from the low frequency limit of Fig. 8 because the former is modeled in 3D, whereas the latter is developed in 1D). Fig. 1 *c* illus-

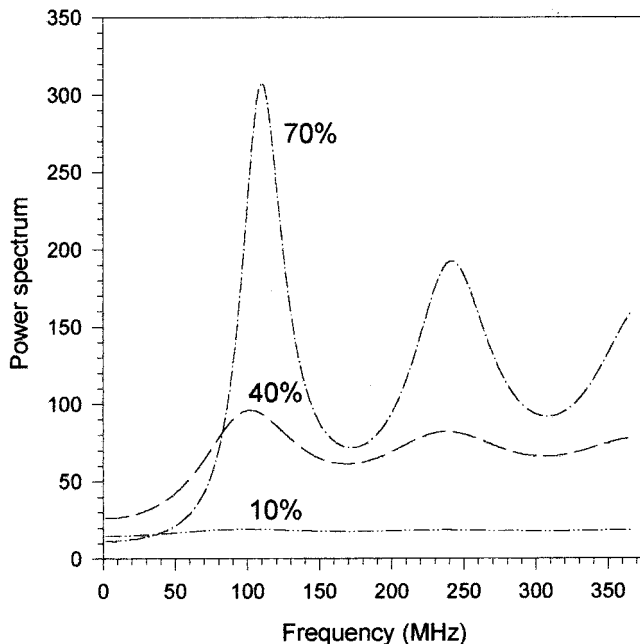


FIGURE 8 Power spectrum of the distribution $N(y)$ computed using the point process approach for hematocrits of 10%, 40%, and 70%. The low-frequency limit of the power spectrum is $H(1 - H)^2/2a$, which is equal to 14.73 at 10% hematocrit, 26.18 at 40% hematocrit, and 11.45 at 70% hematocrit.

trates the power spectrum of the function N based on the packing factor. The mean amplitude of this spectrum is equal to $(H/V)W = \operatorname{var}(n)/\Omega_c$ (see Eqs. 2 and 7). In 1D, the packing factor (W) obtained from the Percus-Yevick pair correlation equation is equal to $(1 - H)^2$ (Twersky, 1987). Thus W , expressed as a function of a and μ , can be written as $W = \mu^2/(2a + \mu)^2$. Moreover, since the cell concentration in 1D ($H/2a$) is equal to $1/(2a + \mu)$, the coefficient $(H/V)W$ is given by $\mu^2/(2a + \mu)^3$. From Eq. 24 with $\omega \rightarrow 0$, the power density spectrum gives the same result, i.e.,

$$\lim_{\omega \rightarrow 0} \{\Phi(j\omega)\} = \frac{\mu^2}{(2a + \mu)^3}. \quad (26)$$

Thus we showed here that the modeling of $N(y)$ based on the point process theory is equivalent to the packing factor approach, at low frequencies. Furthermore, considering that $\lim_{\omega \rightarrow \infty} \{\Phi(j\omega)\} = 1/(\mu + 2a)$, the packing factor can be expressed as the ratio of $\lim_{\omega \rightarrow 0} \{\Phi(j\omega)\}/\lim_{\omega \rightarrow \infty} \{\Phi(j\omega)\}$.

To better understand the effect of these two modeling approaches on the backscattered power, simulations as a function of the frequency were performed in 1D. The results are presented in Fig. 9 for a hematocrit of 40%. Both curves were obtained using the PSF $T(y)$ of Eq. 19 and the sphere

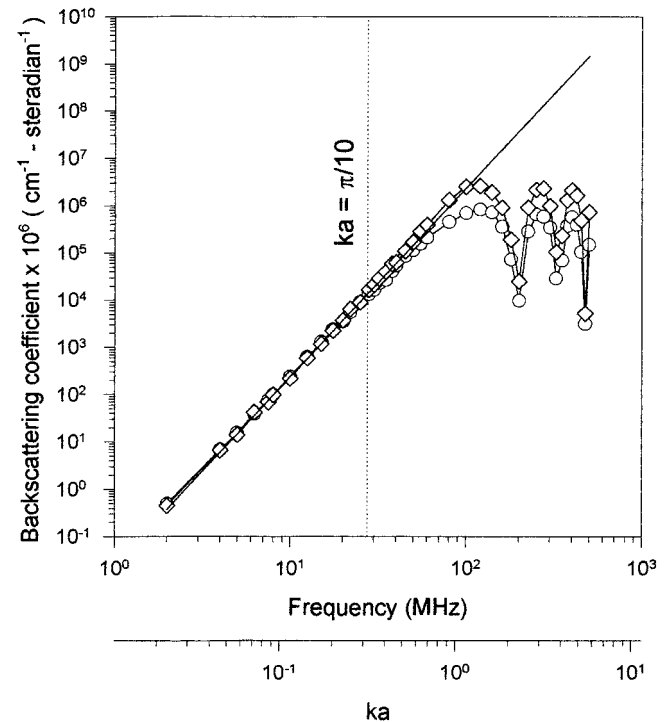


FIGURE 9 Backscattering coefficient as a function of the frequency at 40% hematocrit. —, The theoretical fourth-power frequency dependence. O, 1D simulation results obtained by using the packing factor method to compute $N(y)$; ◇, the results obtained with the point process approach. Both results were computed using the spherical scatterer prototype, and they are expressed in terms of mean \pm one standard error ($n = 100$ simulations). The parameters ka corresponding to the frequency scale are also indicated on the x axis, where k is the wavenumber and a is the radius of the scatterers.

as the cell prototype function (Eq. 20). The diamonds correspond to the simulations performed with the point process theory, and the circles correspond to the packing factor approach ($\text{var}(n) = \Omega_c(H/V)W$, with $W = (1 - H)^2$ in 1D). The results obtained from the two different definitions of $N(y)$ are very similar. Even if the function N obtained using the new approach oscillates at high frequencies, the oscillations of the backscattered power for $ka > \pi/10$ are mostly determined by the cell function (C) defined in Eq. 20.

Theoretical predictions

The current model predicts that for perfectly ordered scatterers (null variance), the backscattered power is effectively null, except for some frequencies. It is well known that regularly spaced scatterers result, in the frequency domain, in a set of regularly spaced impulses. Thus, the backscattered power is null, unless the repetition frequency of the pulses falls within the system bandwidth. It can easily be shown that the repetition frequency, in Hz, is equal to $f_{\text{rep}} = c\alpha/2$, where c is the sound velocity in the medium and α is the average pulse density. Thus, the backscattering is almost zero, unless the frequency of the transducer f is a multiple of f_{rep} . Of course, for scatterers the size of a RBC, the repetition frequency is very high (i.e., over 100 MHz), and the backscattered power is zero for scatterers separated by the same distance and a transducer frequency below 100 MHz.

Future work

In the present study, all simulations were done using identical scatterers. It is possible and it would be interesting to improve this model to allow polydispersity in scatterer sizes. Furthermore, nothing was done to avoid the overlap of very close scatterers. Previous simulation models did implement the modeling of nonoverlapping RBC positions (Zhang et al., 1994; Lim et al., 1996). For a given spatial distribution of the scatterers, mean number and variance, the overlap of the scatterers should not affect the results because the transducer cannot resolve individual scatterers. It would also be interesting to introduce the hypothesis of the hybrid approach, which suggests the voxel as the scattering unit (Lim et al., 1996). In this case, it would not be necessary to define every single scatterer in the sample volume when applying the system-based model presented in this study. It would also be relevant to allow for the motion of RBCs, a property that can be included in the model (Meunier and Bertrand, 1995). Finally, it may be of interest to model the point process approach in 2D or 3D, especially for studying high frequencies.

CONCLUSION

The results presented in this study contribute to a better understanding of the basic mechanisms of ultrasound backscattering and demonstrate that the system-based model is

valid, flexible, and efficient in simulating the ultrasonic signal backscattered by RBCs suspended in a saline solution. This model can be used to simulate Rayleigh as well as non-Rayleigh scattering, as opposed to most theoretical models developed in the literature (Angelsen, 1980; Mo and Cobbold, 1986, 1992; Twersky, 1987; Bascom and Cobbold, 1995), which are limited to the case of Rayleigh scattering. The model confirms that the backscattered signal power is proportional to the variance of the local RBC concentration, although it is still not well known how the size distribution, the shape, and the flow conditions affect this variance. The results also demonstrate that the backscattered power is proportional to the square of the volume of the scatterers weighted by the packing factor, at a constant scatterer number density. On the other hand, the power was shown to be linearly proportional to the volume of the scatterers when the hematocrit (volume concentration) is kept constant. A new approach to modeling the spatial arrangement of the scatterers suggests a frequency dependence of this function. This approach is promising but is currently being developed only in 1D. In future studies, it would also be interesting to model RBC aggregation and flow turbulence, which are expected to affect the variance in the spatial distribution of the scatterers.

APPENDIX: A SYSTEM-BASED INTERPRETATION OF THE STRUCTURE FACTOR

The structure factor $W(k, (\hat{r}_i - \hat{r}_o))$, defined in Eq. 3, can be written, for backscattering measurements, in which case $\hat{r}_i = -\hat{r}_o$, as

$$W(\tilde{k}) = 1 + \rho \int [g(R_p) - 1] e^{-j\tilde{k} R_p} dR, \quad (\text{A1})$$

where $\tilde{k} = 2k$.

In this case, the structure factor can be interpreted as being a line of the 3D Fourier transform of the total correlation function $[g(R_p) - 1]$, the line being in the direction of the incident wave. This can easily be seen by considering a particular case, that of an incident plane wave in the y direction of a Cartesian coordinate system (x, y, z) . Indeed with this, Eq. A1 becomes

$$W(\tilde{k}) = 1 + \rho \iiint [g(x, y, z) - 1] e^{-j\tilde{k}y} dx dy dz. \quad (\text{A2})$$

Thus, it can be seen that the structure factor is proportional to a 1D Fourier transform of the projection, on the propagation axis, of the 3D total correlation function. By the Fourier slice theorem, this 1D Fourier transform is a line of the 3D spectrum of $[g(R_p) - 1]$.

The structure factor can also be described in terms of the microscopic density distribution N , which is a set of Dirac pulses representing the scatterers' spatial distribution:

$$N(x, y, z) = \sum_{i=1}^M \delta(x - x_i, y - y_i, z - z_i), \quad (\text{A3})$$

where (x_i, y_i, z_i) are the coordinates of the i th scatterer, and M is the number of scatterers. Let r_i be the location of the i th scatterer; the Fourier transform

of this function is equal to

$$N(\tilde{k}) \propto \sum_{i=1}^M \exp(-j\tilde{k}r_i). \quad (\text{A4})$$

The following demonstration is intended to show that

$$W(\tilde{k}) \propto \frac{1}{M} \langle N(\tilde{k})N(-\tilde{k}) \rangle, \quad (\text{A5})$$

which is equivalent to

$$\begin{aligned} W(\tilde{k}) &\propto \frac{1}{M} \left\langle \sum_i \sum_j e^{-j\tilde{k}(r_i-r_j)} \right\rangle \\ &= \frac{1}{M} \left\langle \sum_{i=j} e^{-j\tilde{k}(r_i-r_j)} \right\rangle + \frac{1}{M} \left\langle \sum_{i \neq j} e^{-j\tilde{k}(r_i-r_j)} \right\rangle. \end{aligned} \quad (\text{A6})$$

The first term of this last equation is equal to 1. Considering $R_p = r_i - r_j$, the second term is an average of a sum over all pairs of particles of the function $\exp(-j\tilde{k}R_p)$. Like any average, it can be rewritten as an integral of $\exp(-j\tilde{k}R_p)$ with the probability that two particles are located at r_i and r_j , which is given by $\rho^2[g(R_p) - 1]$. Thus A6 becomes

$$\begin{aligned} W(\tilde{k}) &= 1 + \frac{1}{M} \rho^2 \int d\mathbf{r}_i \int [g(R_p) - 1] e^{-j\tilde{k}R_p} d\mathbf{R} \\ &= 1 + \rho \int [g(R_p) - 1] e^{-j\tilde{k}R_p} d\mathbf{R}. \end{aligned} \quad (\text{A7})$$

This last equation is equivalent to Eq. A2. For more details on this topic, refer to Friedman (1985) or <http://www.plmsc.psu.edu/~www/matsc597c-1997/systems/Lecture3/node2.html>.

The authors acknowledge Mr. Guy Charron for helpful discussions.

This work was supported by a studentship from the Natural Sciences and Engineering Research Council of Canada (IF), by a research scholarship from the Fonds de la Recherche en Santé du Québec (GC), by operating grants from the Medical Research Council of Canada (#MT-12491) and the Heart and Stroke Foundation of Québec (GC), and by a team infrastructure grant from the Fonds Concertés pour l'Aide à la Recherche of Québec (MB).

REFERENCES

- Angelsen, B. A. J. 1980. A theoretical study of the scattering of ultrasound from blood. *IEEE Trans. Biomed. Eng.* BME-27:61–67.
- Bamber, J. C., and R. J. Dickinson. 1980. Ultrasonic B-scanning: a computer simulation. *Phys. Med. Biol.* 25:463–479.
- Bascom, P. A. J., and R. S. C. Cobbold. 1995. On a fractal packing approach for understanding ultrasonic backscattering from blood. *J. Acoust. Soc. Am.* 98:3040–3049.
- Berger, N. E., R. J. Lucas, and V. Twersky. 1991. Polydisperse scattering theory and comparisons with data for red blood cells. *J. Acoust. Soc. Am.* 89:1394–1401.
- Christopher, D. A., P. N. Burns, B. G. Starkoski, and F. S. Foster. 1997. A high-frequency pulsed-wave Doppler ultrasound system for the detection and imaging of blood flow in the microcirculation. *Ultrasound Med. Biol.* 23:997–1015.
- Ferrara, K. W., B. G. Zagar, J. B. Sokil-Melgar, R. H. Silverman, and I. M. Aslanidis. 1996. Estimation of blood velocity with high frequency ultrasound. *IEEE Trans. Ultrason. Ferroelec. Freq. Cont.* 43:149–157.

- Friedman, H. L. 1985. *A Course in Statistical Mechanics*. Prentice-Hall, Englewood Cliffs, NJ.
- Gough, W., H. F. Routh, and R. P. Williams. 1988. Weak reflection of a wave by a one-dimensional array of randomly spaced elements, with reference to the scattering of ultrasound by blood. *Phys. Med. Biol.* 33:793–804.
- Ishimaru, A. 1978. Scattering and absorption of a wave by a single particle. In *Wave Propagation and Scattering in Random Media*. A. Ishimaru, editor. Academic Press, New York, San Francisco, London. 9–27.
- Kuo, I. Y., and K. K. Shung. 1994. High frequency ultrasonic backscatter from erythrocyte suspension. *IEEE Trans. Biomed. Eng.* 41:29–34.
- Lim, B., P. A. J. Bascom, and R. S. C. Cobbold. 1996. Particle and voxel approaches for simulating ultrasonic backscattering from tissue. *Ultrasound Med. Biol.* 22:1237–1247.
- Lucas, R. J., and V. Twersky. 1987. Inversion of ultrasonic scattering data for red blood cell suspensions under different flow conditions. *J. Acoust. Soc. Am.* 82:794–799.
- Meunier, J., and M. Bertrand. 1995. Echographic image mean gray level changes with tissue dynamics: a system-based model study. *IEEE Trans. Biomed. Eng.* 42:403–410.
- Mo, L. Y. L., and R. S. C. Cobbold. 1986. A stochastic model of the backscattered Doppler ultrasound from blood. *IEEE Trans. Biomed. Eng.* BME-33:20–27.
- Mo, L. Y. L., and R. S. C. Cobbold. 1992. A unified approach to modeling the backscattered Doppler ultrasound from blood. *IEEE Trans. Biomed. Eng.* 39:450–461.
- Mo, L. Y. L., I. Y. Kuo, K. K. Shung, L. Ceresne, and R. S. C. Cobbold. 1994. Ultrasound scattering from blood with hematocrits up to 100%. *IEEE Trans. Biomed. Eng.* 41:91–95.
- Morse, P. M., and K. U. Ingard. 1968. *The scattering of sound*. In *Theoretical Acoustics*. P. M. Morse and K. U. Ingard, editors. McGraw-Hill, New York, St. Louis, San Francisco. 400–446.
- Papoulis, A. 1991. *Probability Random Variables, and Stochastic Processes*. McGraw-Hill, New York, St. Louis, San Francisco, Auckland.
- Rayleigh, J. W. S. 1945. *Vibrations of solid bodies*. In *Theory of Sound*. Dover Publications, New York. 415–431.
- Routh, H. F., W. Gough, and R. P. Williams. 1987. One-dimensional computer simulation of a wave incident on randomly distributed inhomogeneities with reference to the scattering of ultrasound by blood. *Med. Biol. Eng. Comput.* 25:667–671.
- Routh, H. F., R. P. Williams, and W. Gough. 1989. Weak reflection of ultrasound by elements arranged in the steps of a one-dimensional random walk, with reference to backscatter by blood. *Med. Biol. Eng. Comput.* 27:198–203.
- Shung, K. K. 1982. On the ultrasound scattering from blood as a function of hematocrit. *IEEE Trans. Sonics Ultra.* SU-29:327–331.
- Shung, K. K., I. Y. Kuo, and G. Cloutier. 1993. Ultrasonic scattering properties of blood. In *Intravascular Ultrasound*. J. Roelandt, E. J. Gussenhoven, and N. Bom, editors. Kluwer Academic Publishers, Dordrecht, the Netherlands. 119–139.
- Shung, K. K., R. A. Sigelmann, and J. M. Reid. 1976. Scattering of ultrasound by blood. *IEEE Trans. Biomed. Eng.* BME-23:460–467.
- Shung, K. K., and G. A. Thieme. 1993. *Ultrasonic Scattering in Biological Tissues*. CRC Press, Boca Raton, Ann Arbor, London, Tokyo.
- Shung, K. K., Y. W. Yuan, D. Y. Fei, and J. M. Tarbell. 1984. Effect of flow disturbance on ultrasonic backscatter from blood. *J. Acoust. Soc. Am.* 75:1265–1272.
- Shwedyk, E., R. Balasubramanian, and R. N. Scott. 1977. A nonstationary model for the electromyogram. *IEEE Trans. Biomed. Eng.* BME-24:417–424.
- Turnbull, D. H., B. G. Starkoski, K. A. Harasiewicz, J. L. Semple, L. From, A. K. Gupta, D. N. Sauder, and F. S. Foster. 1995. A 40–100 MHz B-scan ultrasound backscatter microscope for skin imaging. *Ultrasound Med. Biol.* 21:79–88.
- Twersky, V. 1975. Transparency of pair-correlated, random distributions of small scatterers, with application to the cornea. *J. Optical Soc. Am.* 65:524–530.
- Twersky, V. 1987. Low-frequency scattering by correlated distributions of randomly oriented particles. *J. Acoust. Soc. Am.* 81:1609–1618.

- Weng, X., G. Cloutier, P. Pibarot, and L. G. Durand. 1996. Comparison and simulation of different levels of erythrocyte aggregation with pig, horse, sheep, calf, and normal human blood. *Biorheology*. 33:365–377.
- Yuan, Y. W., and K. K. Shung. 1988a. Ultrasonic backscatter from flowing whole blood. II. Dependence on frequency and fibrinogen concentration. *J. Acoust. Soc. Am.* 84:1195–1200.
- Yuan, Y. W., and K. K. Shung. 1988b. Ultrasonic backscatter from flowing whole blood. I. Dependence on shear rate and hematocrit. *J. Acoust. Soc. Am.* 84:52–58.
- Zhang, J., J. L. Rose, and K. K. Shung. 1994. A computer model for simulating ultrasonic scattering in biological tissues with high scatterer concentration. *Ultrasound Med. Biol.* 20:903–913.